Chakraborti, Soumyananda; Korpi, Antti; Kumar, Mantu; Stpień, Piotr; Kostiainen, Mauri A.; Heddle, Jonathan G.

Three-Dimensional Protein Cage Array Capable of Active Enzyme Capture and Artificial Chaperone Activity

Published in:
Nano Letters

DOI:
10.1021/acs.nanolett.9b01148

Published: 01/06/2019

Document Version
Publisher's PDF, also known as Version of record

NANO LETTERS

Letter

Cite This: Nano Lett. 2019, 19, 3918−3924

pubs.acs.org/NanoLett

Three-Dimensional Protein Cage Array Capable of Active Enzyme Capture and Artificial Chaperone Activity

Soumyananda Chakraborti,*[,†] Antti Korpi,[‡] Mantu Kumar,[†,§] Piotr Stępień,[†] Mauri A. Kostiainen,[‡] and Jonathan G. Heddle*[,†]

[†]Bionanoscience and Biochemistry Laboratory, Malopolska Centre of Biotechnology, Jagiellonian University, Gronostajowa 7A, 30-387 Krakow, Poland

[‡]Biohybrid Materials, Department of Bioproducts and Biosystems, Aalto University, FI-00076 Aalto, Finland

[§]Postgraduate School of Molecular Medicine; Żwirki i Wigury 61, 02-091 Warsaw, Poland

Supporting Information

ABSTRACT: Development of protein cages for encapsulation of active enzyme cargoes and their subsequent arrangement into a controllable three-dimensional array is highly desirable. However, cargo capture is typically challenging because of difficulties in achieving reversible assembly/disassembly of protein cages in mild conditions. Herein we show that by using an unusual ferritin cage protein that undergoes triggerable assembly under mild conditions, we can achieve reversible filling with protein cargoes including an active enzyme. We demonstrate that these filled cages can be arrayed in three-dimensional crystal lattices and have an additional chaperone-like effect, increasing both thermostability and enzymatic activity of the encapsulated enzyme.

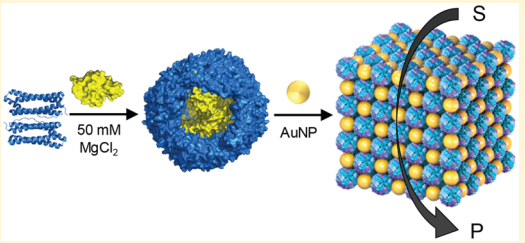

KEYWORDS: *Ferritin, enzyme encapsulation, chaperone activity, ferritin superlattice, 3D enzyme array*

In nature, proteins can self-assemble into a wide variety of large, complex, and highly symmetric architectures including filaments, protein lattices, and symmetric cages,[1] the latter including virus capsids[2] and bacterial microcompartments such as carboxysomes.[3] The majority of protein cages are hollow and spherical (though there are notable exceptions such as vaults,[4] tobacco mosaic virus,[5] and E2[6]). These cages often have icosahedral, octahedral, or tetrahedral symmetry, which plays an important role in controlling their intersubunit interactions.[7,8] In the last two decades, protein cages have been developed extensively, especially as nanocontainers for encapsulation of many cargos including proteins/enzymes.[9] Advantages of encapsulation include increased cargo stability and protection from harsh environmental challenges such as proteases.[10,11] Protein cages can also be used as reaction centers for multienzyme catalysis[12,13] and in many cases can be produced easily in large quantities using recombinant techniques. These features, along with their in-built biocompatibility, make them attractive choices for cell-targeting and drug delivery.[9,14]

Ferritin is one of the most widely used protein cages and is preferred for many applications because of its unique biomineralization ability and high stability.[15] It is a near-ubiquitous protein found in all three domains of life and serves to store iron and protect cells from metal-induced toxicity.[15] Ferritin cages consist of 24 protein subunits, with an outer diameter of approximately 12 nm and an inner cavity of approximately 8 nm and can be isolated as a hollow apo-ferritin lacking the mineralized core.[15] The internal cavity of ferritin has been filled with various materials including nanoparticles, polymers, contrast agents, and proteins (including enzymes) while the exterior has been decorated with numerous molecules including antigens, antibodies, siRNA, and PEG. It has also been used as a constituent of multicomponent nanostructures with lipids[16,17] and has found potential uses in several different medical applications such as bioimaging, cancer therapeutics, and vaccine development.[18−20]

Recently, a new class of ferritins was discovered in archaea, which shows unusual properties such as salt-mediated disassembly[21,22] and high thermal stability.[23] This ability of the ferritin cage to break down when salt conditions are changed is interesting: One potential demerit of most ferritin-based systems has been that the cage subunits are held tightly together by a robust network of noncovalent protein−protein interactions.[15] This means that these ferritin cages spontaneously form and cannot be broken down except under harsh conditions such as very low pH. Typically, the resulting unfolded protein then cannot be easily reassembled.[24] Even ferritins engineered to have better reversible disassembly characteristics require a pH of approximately 2, which may be unsuitable for many cargoes.[25,26]

Generating protein cage based crystals and superlattices from nanoscale building blocks is a field of growing interest and aims to develop new materials based on bottom-up and

Received: March 20, 2019
Revised: May 18, 2019
Published: May 22, 2019

DOI: 10.1021/acs.nanolett.9b01148
Nano Lett. 2019, 19, 3918−3924

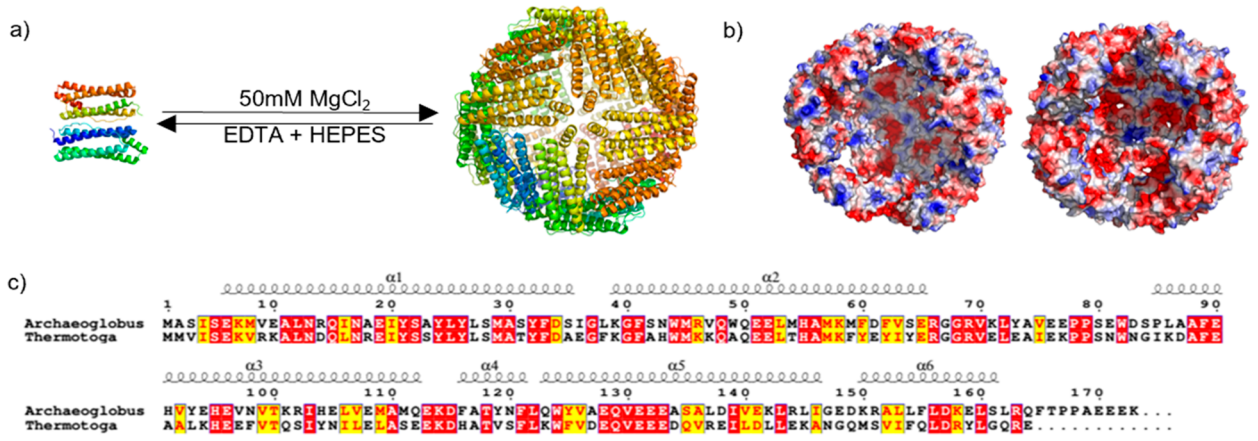

Figure 1. Structure, sequence, and assembly mechanism of two unique archaeal ferritins. (a) Schematic showing TmFtn (PDB ID: 1VLG) assembly in the presence of 50 mM $MgCl_2$ from its individual dimers (dimer shown on left). (b) Electrostatic potential of the lumen of AfFtn (PDB ID: 1S3Q) and TmFtn generated using PyMOL (https://pymol.org/2/).[1] Twelve chains were removed to display the internal cavities of the proteins. Red: -5 kTe^{-1}. Blue: $+5$ kTe^{-1}. (c) Amino acid sequence alignment of TmFtn with AfFtn (http://tcoffee.crg.cat/). In the figure, α-helices are shown as coils, and yellow and red boxes represent similar and identical amino acid residues, respectively.

self-templating techniques.[27] One of the major advantages of using protein cages is that their inner cavities can be packaged with a variety of materials, even including functional enzymes.[27] In this way protein cages could be developed as a general tool for arranging many different proteins in superlattices, including those that may not otherwise be amenable to doing so. To date, higher-order protein cage structures have mostly been generated through utilization of electrostatic interactions between the cage and partner nanoparticles. For example, Kostiainen et al. have shown that *Pyrococcus furiosus* ferritin (PfFtn) and cowpea chlorotic mottle virus (CCMV) cages can be self-assembled into three-dimensional (3D) architectures via electrostatic interactions with gold nanoparticles[28] and subsequently developed several other tools to generate higher-order ferritin structures.[29−32] Recently, Douglas et al. showed that other virus like particles, such as bacteriophage P22, can also be utilized as templates to generate 3D protein cage architectures and demonstrated that such superlattices can be made catalytically active.[33] Very recently, Zhao et al. showed that a simple tuning of aromatic stacking interactions can be used to assemble ferritin into higher-order structures.[34] Though a handful of methods enabling ferritin lattice formation have now been demonstrated, catalytically active versions have not been reported to date but are desirable due to ferritin's widespread use as a nanotechnology tool. A major hurdle has been the difficulty of filling ferritins due to the dissociation and reassociation challenges.

Archaeal ferritin from *Archaeoglobus fulgidus* (AfFtn) offers a partial solution to this problem: it has a unique quaternary structure, assembling into a 24-mer cage with tetrahedral rather than the usual octahedral symmetry found in most other ferritins and has four remarkable triangular pores of ∼45 Å in diameter.[21,35] This allows large cargos to easily enter the cage.[36] Furthermore, AfFtn also shows salt-mediated assembly properties, existing as a simple dimer in low salt and assembling into cages at high salt, providing the potential for a simple and relatively mild salt-based reversible assembly/disassembly. This has been demonstrated by encapsulation of positively charged gold nanoparticles,[37] supercharged GFP and several enzymes linked to supercharged GFP.[36,38] A possible problem with AfFtn that makes it unsuitable for protein or RNA delivery is that the large pore size may make cargo vulnerable to attack from degrading agents for example ribonuclease H and small proteases (e.g., trypsin or α-chymotrypsin). Exclusion by other cargos having higher affinity could also occur. In addition, the large pore may allow the cargo to simply diffuse out of the cavity especially at high electrolyte concentrations where electrostatic interactions are screened. In this work, we have addressed these challenges by developing a novel ferritin that retains salt-mediated assembly/disassembly, but which has a closed shell.

We used *Thermotoga maritima* ferritin (TmFtn; PDB ID: 1VLG), which is one of the few extremophile ferritins whose high-resolution structure is known. TmFtn is structurally similar to other known bacterial and eukaryotic ferritins,[20] consisting of 24 identical subunits forming a convex, closed shell (Figure 1a). It has a molecular weight of about 460 kDa and displays octahedral symmetry but shows salt-sensitive assembly.[22] Despite its structure being known, and its salt-dependent assembly having been noted, TmFtn has never been utilized for cargo encapsulation despite the potential utility offered by its unique mix of characteristics. Filling of protein cages with and retention of cargo is often achieved via electrostatic effects[38] and with a view to using the same approach for filling of TmFtn, we first measured the surface charge distribution of the internal surface in comparison to wild-type AfFtn, which has already been shown able to encapsulate positively supercharged, +36GFP[39] and a number of active enzymes.[36,38] We found that the net charge on the internal lumen of both protein cages (AfFtn and TmFtn) is similarly negative (Figure 1b), as expected given their equivalent *in vivo* roles in iron mineralization. Comparison of the amino acid sequences of AfFtn and TmFtn showed 51% identity and more than 70% similarity (Figure 1c).

TmFtn was next produced and purified (see the Supporting Information for details including Figure S1 for sequence information) followed by characterization as this cage has not been fully characterized to date. TmFtn showed salt-induced assembly in the presence of both monovalent (NaCl) and divalent ($MgCl_2$, $CaCl_2$) metal ions. However, we found that divalent cations are clearly more effective in promoting assembly (Figure S2a). Ferritin cage assembly in the presence of Mg^{2+} was confirmed by dynamic light scattering (DLS),

DOI: 10.1021/acs.nanolett.9b01148
Nano Lett. 2019, 19, 3918−3924

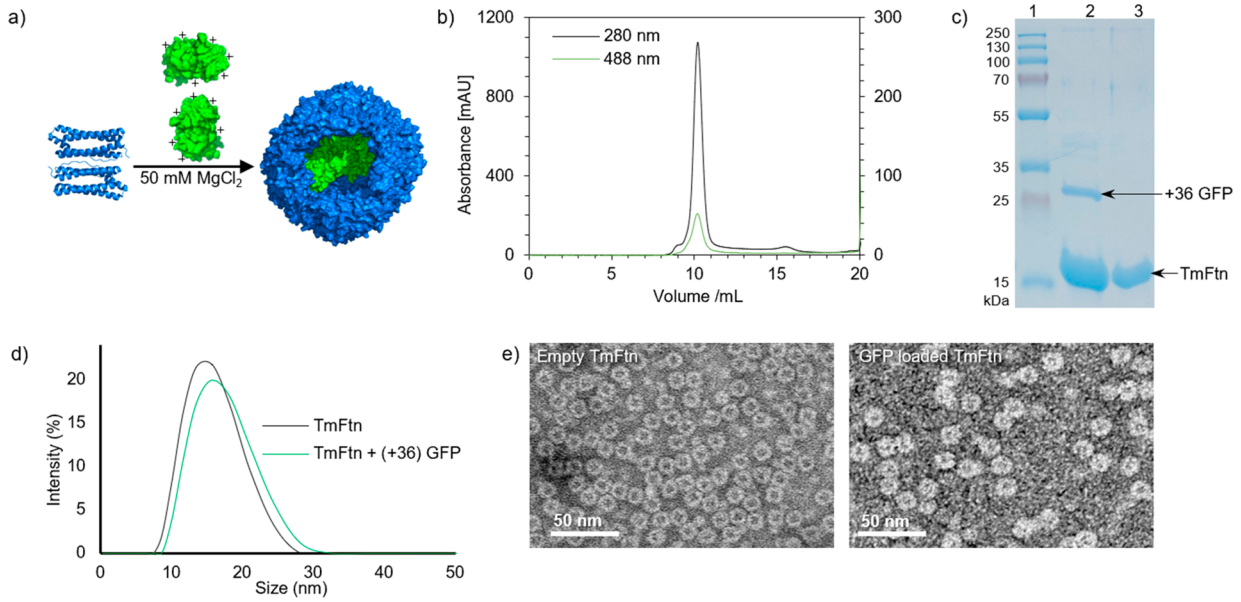

Figure 2. Encapsulation of supercharged GFP inside TmFtn. (a) Schematic showing encapsulation of +36GFP inside the lumen of TmFtn. Dimeric ferritin (left, blue cartoon representation) is assembled in the presence of Mg^{2+} and +36GFP (green, represented by nonsupercharged structure PDB ID: 1EME)) to form the ferritin cage with GFP cargo (right). Ferritin cage and encapsulated GFP are shown in surface representation. (b) SEC profile showing coelution of GFP and ferritin cages. The GFP peak is shown in green. (c) Association of GFP and ferritin further verified using SDS-PAGE. The isolated, post-encapsulation protein cage shows bands corresponding to both GFP and TmFtn (lane 2). Lane 1 and lane 3 represent marker and free TmFtn, respectively (d) DLS showing no significant change in the diameter of ferritin after interaction with GFP, inferring encapsulation. (e) TEM images showing empty (left) and GFP loaded (right) ferritin.

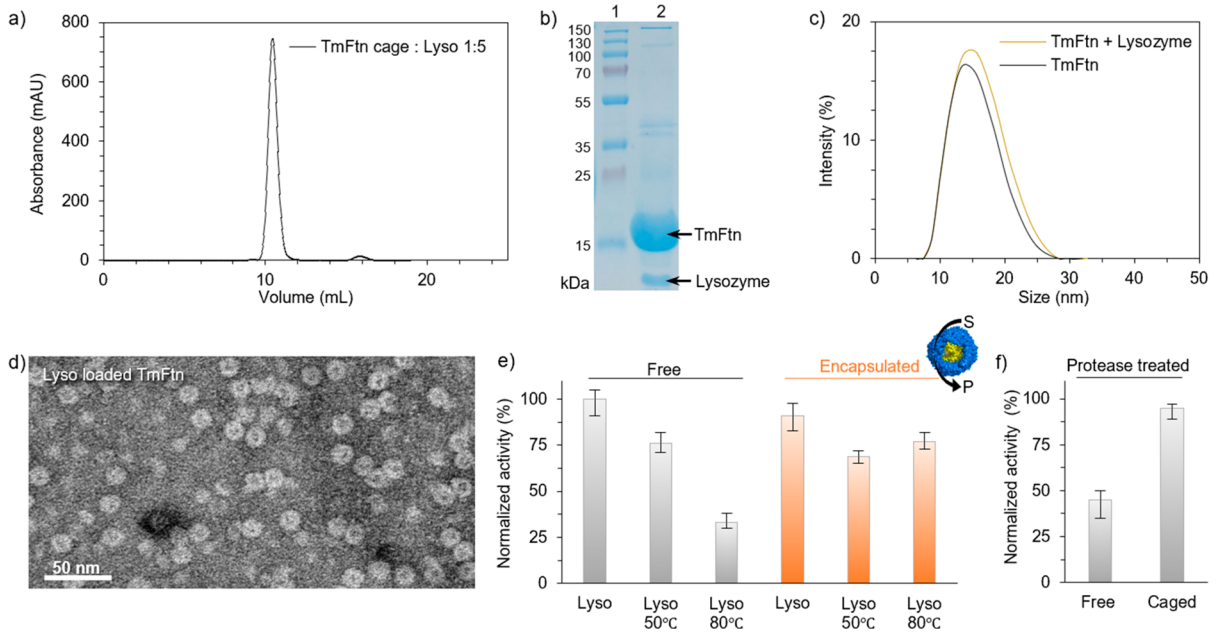

Figure 3. Active lysozyme encapsulation and chaperone-like activity of TmFtn. (a) SEC profile showing lysozyme coelution with TmFtn after encapsulation reaction (for full range of cage:cargo ratios see Figure S5). (b) SDS-PAGE analysis of purified particles after coelution with lysozyme. Lane 1 = protein marker (molecular weights shown on left). Lane 2 = purified particles, clearly showing bands corresponding to lysozyme and TmFtn. (c) DLS of purified particles after the encapsulation reaction ("TmFtn + Lysozyme") compared to empty ferritin cages ("TmFtn") showing no change in the external diameter. (d) TEM image showing particles after lysozyme encapsulation reaction. (e) Comparison of the enzymatic activities of free and encapsulated lysozyme at different temperatures suggesting that TmFtn protects cargo against heat induced denaturation. (f) Effect of trypsin on the activity of encapsulated or free lysozyme showing protection of the encapsulated cargo.

which showed a single, sharp peak corresponding to particles of ~15 nm diameter (Figure S2b). Transmission electron microscopy (TEM) and atomic force microscopy (AFM) confirmed particle quality with the former showing homogeneous particles of diameter 12−14 nm (Figure S2c) and the latter giving a particle height of approximately 12 nm, in line with the solved crystal structure [PDB ID: 1VLG]. Circular dichroism measurements validated the α-helical nature of the protein, adding further evidence that it was correctly folded (Figure S2d). TmFtn is expected to be highly thermostable,

DOI: 10.1021/acs.nanolett.9b01148
Nano Lett. 2019, 19, 3918−3924

but this has never been experimentally demonstrated; therefore, we assessed the thermostability using DLS, which clearly showed no observable aggregation even at the highest temperature tested (95 °C). In contrast, aggregation of AfFtn was observed beginning at ∼70 °C (Figure S3a). Thermostability was further verified by heating at 95 °C for 30 min followed by negative staining and TEM imaging, which showed no significant change in cage morphology (Figure S3a, inset). CD measurements of helical content also showed no change up to 95 °C (Figure S3b). The thermal stability of TmFtn compared to AfFtn was further measured using differential scanning calorimetry (DSC). For TmFtn, no denaturation signal was seen up to the highest temperature used (95 °C). In comparison, AfFtn showed a denaturation transition starting at ∼75 °C and completed by ∼85 °C (Figure S3c). We also observed that TmFtn showed little evidence of aggregation over a pH range of 5−10 (Figure S3d).

As TmFtn carries an overall negative charge on its interior surface (Figure 1b), we hypothesized that it would be able to encapsulate a positively charged cargo (Figure 2a). To test this, we selected +36GFP (pI 10.4)[36] as a suitable cargo due to its charge and ease of detection. For efficient encapsulation, we followed a protocol previously developed by Tetter et al.,[38] with minor modifications. The respective proteins were incubated overnight at 4 °C, and size exclusion chromatography (SEC) showed that protein cargos coeluted with assembled cage (Figure 2b). The coeluting fractions were collected and subjected to SDS-PAGE, which clearly showed the presence of both +36GFP and TmFtn (Figure 2c).

The fractions from SEC in which both cage and cargo protein were present were analyzed by DLS (Figure 2d, Figure S4a), which showed almost no increase in particle hydrodynamic radius, further indicating that the cargo was indeed encapsulated rather than attached nonspecifically to the exterior of the cage. Fractions from SEC containing both ferritin and cargo were visualized using transmission electron microscopy (TEM). TEM confirms lack of protein on the exterior of ferritin cages (Figure 2e). TEM images of ferritin without cargo (Figure 2e, left) show a black core typical of heavy atom staining, while ferritin with protein cargo (Figure 2e, right) shows a whiter core, expected if cargo is present and excludes stain, though care must be taken in overinterpreting negative stain TEM results of encapsulation for such small cargo particles.

Having successfully encapsulated supercharged GFP, we next attempted to encapsulate an active enzyme. We selected lysozyme for this purpose as it shares an isoelectric point (pI ∼ 11)[40] similar to that of +36GFP. The encapsulation procedure was almost identical to that used for +36GFP. After overnight encapsulation a single peak was isolated from SEC (Figure 3a). Subjecting this isolated peak to SDS-PAGE showed the presence of protein bands corresponding to both lysozyme and TmFtn (Figure 3b). The same fraction was also subjected to DLS analysis (Figure 3c, Figure S4a), which showed no apparent increase in particle hydrodynamic radius after encapsulation. Taken together, these results suggest that the cargo was indeed encapsulated rather than attached nonspecifically to the exterior of the cage. The same SEC fraction was visualized using TEM, which showed no visible protein on the exterior of the ferritin cage and a less dark interior, again suggestive of encapsulated cargo (Figure 3d). It has been observed that some protein cages were highly stable, protecting their cargoes from challenges such as heat and proteases.[11,38] To see if this was true in our case, we tested the effect on the cargo of a range of temperatures over which the protein cage is known to be stable. We found that over the range tested (25−80 °C) the encapsulated lysozyme was active and, surprisingly, showed very high activity at 80 °C, whereas the free enzyme showed significantly decreased activity at higher temperatures (Figure 3e), as expected given the denaturation temperature of the free enzyme, which is known to be approximately 75 °C.[40] Such a thermo-protective effect on protein structure/function has been reported for an enzyme encapsulated inside AfFtn[38] as well as for cargoes in other protein cages such as peptidase E in Qβ.[11] We also checked the protease sensitivity of free and encapsulated lysozyme in the presence of trypsin and found that free lysozyme was more susceptible to digestion compared to the encapsulated enzyme with a correspondingly reduced activity (Figure 3f).

After successful encapsulation experiments, next we quantified the amount of protein/enzyme loaded inside TmFtn. For +36GFP this was determined spectrophotometrically, and we found an average of ∼4 GFPs loaded inside TmFtn under the optimized conditions (Figure S5a) consistent with previous findings for GFP encapsulation by AfFtn.[38] Quantitation of lysozyme loading is more challenging as it lacks any characteristic spectroscopic signature. We used both densitometric analysis of SDS-PAGE gel and analytical SEC, which suggested ∼5 lysozyme molecules inside each TmFtn cage (Figure S5b−g), though it should be noted that this quantitation method is likely to be less accurate. These results are consistent with the interior volume of TmFtn, which we calculated to be 228 794 Å^3.[41] Considering a GFP volume of approximately 35 000 Å^3 and lysozyme volume of 18 000 Å^3, we can calculate a theoretical maximum capacity of ∼7 GFP and ∼13 lysozyme molecules per cage. During cargo encapsulation we observed precipitation at lower ionic strength (10−25 mM $MgCl_2$) for both lysozyme and +36GFP, particularly at higher guest to host ratios. Most likely the cationic protein is binding several ferritins together to form higher-order structures. To further verify cargo encapsulation is solely driven by electrostatic interactions, we used two different charged GFPs. In both cases encapsulation was performed using the same protocol as used for +36GFP. SEC results revealed that both wild-type and −21GFP did not coelute with TmFtn (Figure S5h), confirming our hypothesis that TmFtn cargo encapsulation is purely electrostatic in nature.

The disassembly of TmFtn cage and cargo release was also studied, by altering salt and EDTA concentrations. We hypothesized that EDTA can chelate divalent metal cations including Mg^{2+} and expected its addition to result in disassembly of the TmFtn cage, releasing cargo (Figure S6a). +36GFP-encapsulated TmFtn cage was preincubated overnight with 100 mM EDTA and the sample passed through a SEC column already equilibrated with 100 mM EDTA. In these conditions the TmFtn cage completely dissociated, as evidenced by the disappearance of the peak corresponding to the 24mer cage, which usually appears at approximately 10 mL of elution. A new peak at around 16 mL (lower molecular weight) was observed (due to ferritin dissociation) along with a peak corresponding to GFP, indicating cargo release (Figure S6b). Disassembly of the system was further verified using DLS, which showed that in the presence of EDTA, TmFtn cage spontaneously disassembles into dimers, as evidenced by a decrease in particle size (Figure S6c). During disassembly

DOI: 10.1021/acs.nanolett.9b01148
Nano Lett. 2019, 19, 3918−3924

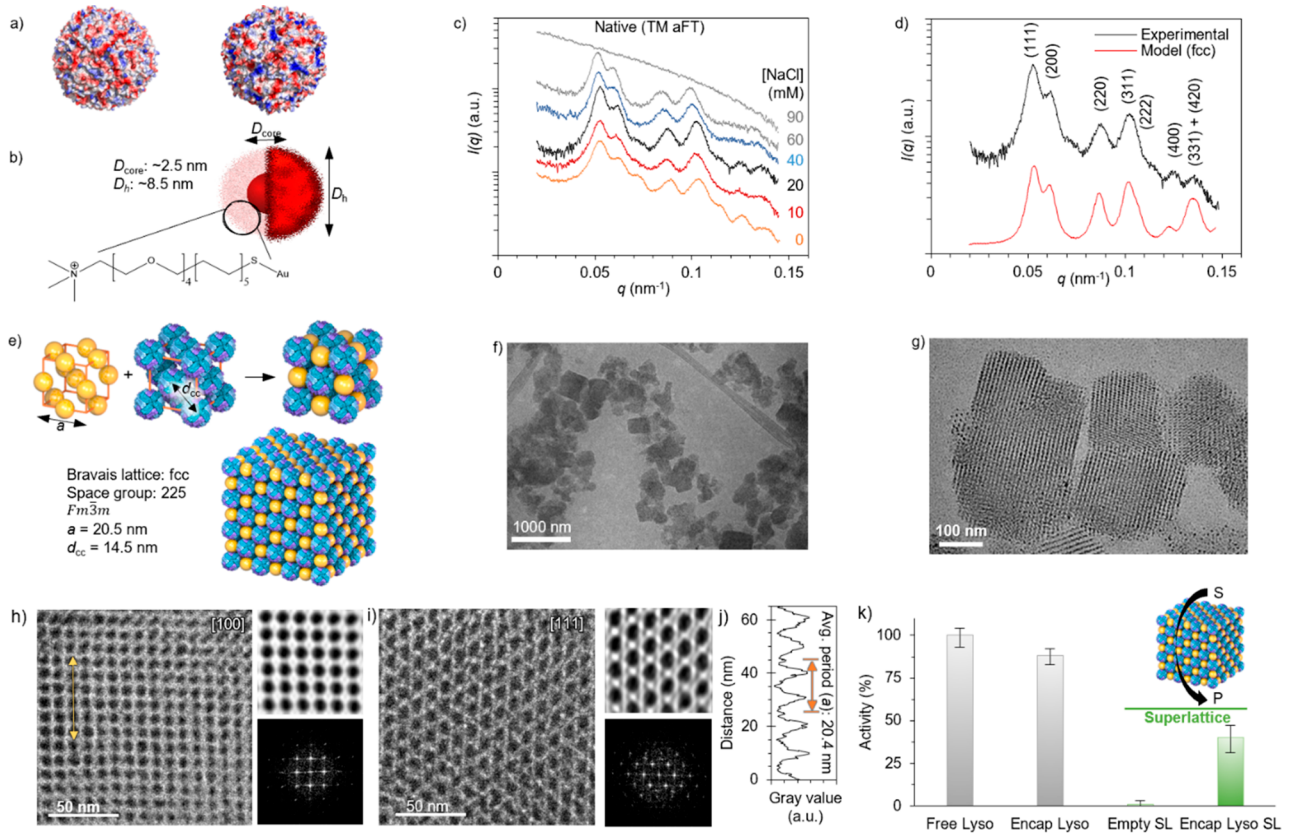

Figure 4. Superlattice formation. (a) Electrostatic surface representations of TmFtn and PfFtn (PDB IDs: 1VLG and 2JD7, respectively) viewed along 3-fold axes. Red: −5 kTe^{-1}. Blue: +5 kTe^{-1}. (b) Cartoon representation of gold nanoparticle with linker. D_{core} was determined using TEM and D_h by DLS. (c) Azimuthally integrated SAXS curves measured from lysozyme-encapsulated TmFtn−AuNP superlattices formed at different NaCl concentrations. (d) Miller indexed curves for the sample formed at 20 mM NaCl compared to a calculated fcc model. (e) Schematic representation of the particle packing. The particles adopt an interpenetrating fcc (NaCl-type) structure with a lattice constant of 20.5 nm. Schemes show the unit cells (outlined with an orange frame) with AuNPs alone, ferritins alone, and their combination. The large complex shows the 3 × 3 unit cell. (f) Low-magnification cryo-TEM image of the formed TmFtn−AuNP crystal lattices, displaying their arrangement into particles 200−300 nm in size and (g) high-resolution image of multiple small crystallites shown in random orientations. (h) TmFtn−AuNP lattice viewed approximately along the [100] projection axis and (i) approximately along the [111] projection axis. Panels show the cryo-TEM image (left), filtered inverse Fourier transform from selected Fourier components (top right), and fast Fourier transform image (bottom right). (j) Integrated profile along the yellow line in panel h yielding an average period (*a*) of 20.4 nm. (k) Activity assay showing that the lysozyme-encapsulated ferritin superlattice is enzymatically active compared to an empty lattice of the same ferritin but is less active than similar concentrations of free enzyme or encapsulated enzyme not in a lattice.

some portion of the protein nonspecifically adsorbed on dialysis membrane filters, which we cannot recover; we believe that is the reason for the observed decreased intensity of the protein signal in the DLS profile. Finally, native PAGE was used to validate the DLS data; we ran both the cage and dimer along with marker protein. Fully formed assemblies gave the expected band corresponding to a cage of approximately 480 kDa whereas cage incubated with EDTA gave predominantly a band corresponding to the dimer (approximately 40 kDa; Figure S6d). We also studied disassembly of TmFtn in the absence of EDTA, by washing the protein in EDTA-free buffer. This can result in some cage disassembly but is much less efficient and requires repeated washing (Figure S7a−f).

Generation of ferritin superlattices has previously been reported using different dendrimer/nanoparticle systems including AuNP.[28] To date this has been carried out using exclusively PfFtn as a building block, which cannot be used for enzyme encapsulation due to difficulties in achieving subunit dissociation with mild conditions, as discussed. Having achieved enzyme encapsulation in TmFtn, we next attempted to form superlattices. As a guide, we compared TmFtn and PfFtn and found that both proteins have almost identical isoelectric points (pI ∼ 4.8). As it is known that the 3-fold axis of ferritin is likely the key area for interactions with linkers that drive superlattice formation,[28] we also compared charge distribution around this axis and found some similarity between TmFtn and PfFtn (Figure 4a).

After successful enzyme encapsulation, we aimed to generate binary crystals with cargo-encapsulated TmFtn and gold nanoparticles.[28−32] After several rounds of screening, we found gold nanoparticles (AuNP) to be the most successful. The AuNP used in this study has a core size of 2.5 nm and possesses a highly positively charged surface ligand (Figure 4b). Titration of AuNPs against a constant amount of TmFtn showed that at the concentrations used, all ferritin was incorporated into the superlattice (Figure S8). Superlattice formation was monitored using small-angle X-ray scattering (SAXS), and the process was optimized by altering the concentration of the monovalent salt (NaCl) (Figure 4c−e). In NaCl concentrations ranging between 0 and 100 mM, TmFtn−AuNP complexes were found to arrange into crystal lattices with interpenetrating face-centered cubic (fcc)

DOI: 10.1021/acs.nanolett.9b01148
Nano Lett. 2019, 19, 3918−3924

structure of both particles. The intense $(hkl) = (111)$ signal can be seen at $q = 0.053$ Å^{-1}, and the next clear signals at 0.062, 0.087, and 0.103 Å^{-1}. When the $q = 0.053$ Å^{-1} position is given the value 1, the following signals fall in positions $\sqrt{(4/3)}$, $\sqrt{(8/3)}$, and $\sqrt{(11/3)}$, which correspond to the planes (200), (220), and (311) in the FCC model (space group $Fm\bar{3}m$, number 225). The most distinct scattering pattern was obtained at 20 mM salt concentration. The lattice constant of all the obtained crystals was 20.5 nm regardless of the NaCl concentration. At 90 mM NaCl the screening effect of the salt is increased to such a level that electrostatic interactions between the particles are lost and higher-order structures are not formed. We further verified lattice formation by cryo-TEM, which clearly shows that TmFtn formed a fcc lattice in the presence of AuNP when mixed in a 1:1 ratio (Figure 4f–j).

Finally, as the TmFtn in the superlattices contained encapsulated lysozyme, we measured its enzymatic activity. We found the superlattice to be enzymatically active as assessed by an assay that monitors the degradation of fluorescently labeled substrate (EnzChek lysozyme assay)[42] (Figure 4k). However, there is a drop in activity of around 2-fold compared to the activity of encapsulated enzyme not in a lattice, possibly reflecting decreased ability of substrate to reach buried target.

To test the hypothesis that the 3-fold axis is the key area for interactions with the AuNPs leading to superlattice formation, we used AfFtn, which, because of its unusual tetrahedral symmetry, does not have filled 3-fold axes. Instead, these are occupied by four large pores (Figure 5a).[20,38]

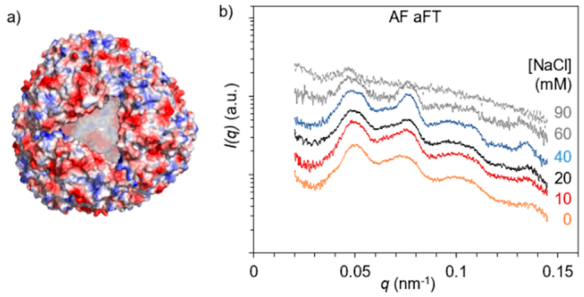

Figure 5. AfFtn does not form superlattices. (a) Electrostatic surface representation of 3-fold axis of AfFtn (PDB ID: 1S3Q). AfFtn contains pores at the 3-fold axis location. (b) Azimuthally integrated SAXS curves measured from AfFtn–AuNP complexes at different NaCl concentrations.

When this protein is subject to lattice-forming experiments under the same conditions as TmFtn, no lattice structures (as shown by SAXS) are observed, and this is true over a range of salt concentrations (Figure 5b). This may be expected if lattice formation is via interaction of AuNPs with charged patches at the 3-fold axis.

In this work we have addressed the major challenge faced when trying to encapsulate cargoes in ferritins. This is the fact that while closed shell (octahedral) ferritins generally have the most robust physicochemical characteristics, they are difficult to disassemble and reassemble. This makes them difficult to fill. Conversely, tetrahedral ferritins can be easily filled due to the large holes in their surface but run the risk of losing cargo through diffusion effects or through digestion by degrading enzymes. Here we have solved this conundrum by demonstrating successful cargo encapsulation in TmFtn. We find that TmFtn is very efficient in forming complexes with positively charged guest proteins within its naturally negatively charged lumen and that this can be achieved by a simple in vitro mixing approach. Finally, we showed that TmFtn carrying an active enzyme can be assembled into a crystalline lattice that retains enzymatic activity. We anticipate that the ability to utilize a widely used "bionano" building block such as ferritin to encapsulate and arrange active enzymes in ordered arrays may prove useful for future biotechnological or biomedical application.

■ ASSOCIATED CONTENT

Supporting Information

The Supporting Information is available free of charge on the ACS Publications website at DOI: 10.1021/acs.nanolett.9b01148.

Figures of TmFtn assembly and ferritin cage biophysical characterization, details of the mechanism of cargo encapsulation, loading efficiency and disassembly of cage; autocorrelation curves correspond to TmFtn encapsulation measured using DLS and sequence of protein constructs used in this study; details of materials and methods used in this study and characterization of free and encapsulated ferritin particles (PDF)

■ AUTHOR INFORMATION

Corresponding Authors

*E-mail: soumyananda.chakraborti@uj.edu.pl.
*E-mail: jonathan.heddle@uj.edu.pl.

ORCID

Mauri A. Kostiainen: 0000-0002-8282-2379
Jonathan G. Heddle: 0000-0003-0994-9928

Notes

The authors declare no competing financial interest.

■ ACKNOWLEDGMENTS

S.C. and M.K. were supported from the Homing programme of the Foundation for Polish Science cofinanced by the European Union under the European Regional Development Fund, grant No. Homing/2017-3/22 awarded to S.C. P.S. and J.G.H. were funded by the Team Programme of the Foundation for Polish Science cofinanced by the European Union under the European Regional Development Fund (TEAM/2016-3/23) awarded to J.G.H. Financial support from the Academy of Finland (Grants 308578, 303804, 273645, 267497, 272579) and Sigrid Juselius Foundation is gratefully acknowledged. The research made use of the instrumentation of Aalto University Nanomicroscopy Center (Aalto-NMC).

■ REFERENCES

(1) Luo, Q.; Hou, C.; Bai, Y.; Wang, R.; Liu, J. Protein Assembly: Versatile Approaches to Construct Highly Ordered Nanostructures. *Chem. Rev.* **2016**, *116* (22), 13571–13632.

(2) Flenniken, M. L.; Uchida, M.; Liepold, L. O.; Kang, S.; Young, M. J.; Douglas, T. A Library of Protein Cage Architectures as Nanomaterials. *Curr. Top. Microbiol. Immunol.* **2009**, *327*, 71–93.

(3) Hagen, A. R.; Plegaria, J. S.; Sloan, N.; Ferlez, B.; Aussignargues, C.; Burton, R.; Kerfeld, C. A. Vitro Assembly of Diverse Bacterial Microcompartment Shell Architectures. *Nano Lett.* **2018**, *18* (11), 7030–7037.

(4) Tanaka, H.; Kato, K.; Yamashita, E.; Sumizawa, T.; Zhou, Y.; Yao, M.; Iwasaki, K.; Yoshimura, M.; Tsukihara, T. The Structure of

DOI: 10.1021/acs.nanolett.9b01148
Nano Lett. 2019, 19, 3918–3924

Rat Liver Vault at 3.5 Angstrom Resolution. *Science* **2009**, *323* (5912), 384−388.
(5) Vernekar, A. A.; Berger, G.; Czapar, A. E.; Veliz, F. A.; Wang, D. I.; Steinmetz, N. F.; Lippard, S. J. Speciation of Phenanthriplatin and Its Analogs in the Core of Tobacco Mosaic Virus. *J. Am. Chem. Soc.* **2018**, *140* (12), 4279−4287.
(6) Molino, N. M.; Neek, M.; Tucker, J. A.; Nelson, E. L.; Wang, S.-W. Viral-Mimicking Protein Nanoparticle Vaccine for Eliciting Anti-Tumor Responses. *Biomaterials* **2016**, *86*, 83−91.
(7) Berger, B.; Shor, P. W.; Tucker-Kellogg, L.; King, J.; Rudnick, J. Local Rule-Based Theory of Virus Shell Assembly. *Proc. Natl. Acad. Sci. U. S. A.* **1994**, *91* (16), 7732−7736.
(8) Diaz, D.; Care, A.; Sunna, A. Bioengineering Strategies for Protein-Based Nanoparticles. *Genes* **2018**, *9* (7), 370.
(9) Wen, A. M.; Steinmetz, N. F. Design of Virus-Based Nanomaterials for Medicine, Biotechnology, and Energy. *Chem. Soc. Rev.* **2016**, *45* (15), 4074−4126.
(10) Wilkerson, J. W.; Yang, S.-O.; Funk, P. J.; Stanley, S. K.; Bundy, B. C. Nanoreactors: Strategies to Encapsulate Enzyme Biocatalysts in Virus-like Particles. *New Biotechnol.* **2018**, *44*, 59−63.
(11) Fiedler, J. D.; Brown, S. D.; Lau, J. L.; Finn, M. G. RNA-Directed Packaging of Enzymes within Virus-like Particles. *Angew. Chem., Int. Ed.* **2010**, *49* (50), 9648−9651.
(12) Jordan, P. C.; Patterson, D. P.; Saboda, K. N.; Edwards, E. J.; Miettinen, H. M.; Basu, G.; Thielges, M. C.; Douglas, T. Self-Assembling Biomolecular Catalysts for Hydrogen Production. *Nat. Chem.* **2016**, *8* (2), 179−185.
(13) Minten, I. J.; Claessen, V. I.; Blank, K.; Rowan, A. E.; Nolte, R. J. M.; Cornelissen, J. J. L. M. Catalytic Capsids: The Art of Confinement. *Chem. Sci.* **2011**, *2* (2), 358−362.
(14) Deshayes, S.; Gref, R. Synthetic and Bioinspired Cage Nanoparticles for Drug Delivery. *Nanomedicine* **2014**, *9* (10), 1545−1564.
(15) Jutz, G.; van Rijn, P.; Santos Miranda, B.; Böker, A. Ferritin: A Versatile Building Block for Bionanotechnology. *Chem. Rev.* **2015**, *115* (4), 1653−1701.
(16) Kameta, N.; Masuda, M.; Minamikawa, H.; Mishima, Y.; Yamashita, I.; Shimizu, T. Functionalizable Organic Nanochannels Based on Lipid Nanotubes: Encapsulation and Nanofluidic Behavior of Biomacromolecules. *Chem. Mater.* **2007**, *19* (14), 3553−3560.
(17) Shaw, A.; Benson, E.; Högberg, B. Purification of Functionalized DNA Origami Nanostructures. *ACS Nano* **2015**, *9* (5), 4968−4975.
(18) Georgiev, I. S.; Joyce, M. G.; Chen, R. E.; Leung, K.; McKee, K.; Druz, A.; Van Galen, J. G.; Kanekiyo, M.; Tsybovsky, Y.; Yang, E. S.; Yang, Y. Two-Component Ferritin Nanoparticles for Multimerization of Diverse Trimeric Antigens. *ACS Infect. Dis.* **2018**, *4* (5), 788−796.
(19) Tsukamoto, R.; Godonoga, M.; Matsuyama, R.; Igarashi, M.; Heddle, J. G.; Samukawa, S.; Yamashita, I. Effect of PEGylation on Controllably Spaced Adsorption of Ferritin Molecules. *Langmuir* **2013**, *29* (41), 12737−12743.
(20) Pulsipher, K. W.; Dmochowski, I. J. Ferritin: Versatile Host, Nanoreactor, and Delivery Agent. *Isr. J. Chem.* **2016**, *56* (9−10), 660−670.
(21) Johnson, E.; Cascio, D.; Sawaya, M. R.; Gingery, M.; Schröder, I. Crystal Structures of a Tetrahedral Open Pore Ferritin from the Hyperthermophilic Archaeon Archaeoglobus Fulgidus. *Structure* **2005**, *13* (4), 637−648.
(22) Ceci, P.; Forte, E.; Di Cecca, G.; Fornara, M.; Chiancone, E. The Characterization of Thermotoga Maritima Ferritin Reveals an Unusual Subunit Dissociation Behavior and Efficient DNA Protection from Iron-Mediated Oxidative Stress. *Extremophiles* **2011**, *15* (3), 431−439.
(23) Tatur, J.; Hagedoorn, P.-L.; Overeijnder, M. L.; Hagen, W. R. A Highly Thermostable Ferritin from the Hyperthermophilic Archaeal Anaerobe Pyrococcus Furiosus. *Extremophiles* **2006**, *10* (2), 139−148.
(24) Kim, M.; Rho, Y.; Jin, K. S.; Ahn, B.; Jung, S.; Kim, H.; Ree, M. PH-Dependent Structures of Ferritin and Apoferritin in Solution: Disassembly and Reassembly. *Biomacromolecules* **2011**, *12* (5), 1629−1640.
(25) Yoshizawa, K.; Mishima, Y.; Park, S.-Y.; Heddle, J. G.; Tame, J. R. H.; Iwahori, K.; Kobayashi, M.; Yamashita, I. Effect of N-Terminal Residues on the Structural Stability of Recombinant Horse L-Chain Apoferritin in an Acidic Environment. *J. Biochem.* **2007**, *142* (6), 707−713.
(26) Chen, H.; Zhang, S.; Xu, C.; Zhao, G. Engineering Protein Interfaces Yields Ferritin Disassembly and Reassembly under Benign Experimental Conditions. *Chem. Commun.* **2016**, *52* (46), 7402−7405.
(27) Aumiller, W. M.; Uchida, M.; Douglas, T. Protein Cage Assembly across Multiple Length Scales. *Chem. Soc. Rev.* **2018**, *47* (10), 3433−3469.
(28) Kostiainen, M. A.; Hiekkataipale, P.; Laiho, A.; Lemieux, V.; Seitsonen, J.; Ruokolainen, J.; Ceci, P. Electrostatic Assembly of Binary Nanoparticle Superlattices Using Protein Cages. *Nat. Nanotechnol.* **2013**, *8* (1), 52−56.
(29) Liljeström, V.; Mikkilä, J.; Kostiainen, M. A. Self-Assembly and Modular Functionalization of Three-Dimensional Crystals from Oppositely Charged Proteins. *Nat. Commun.* **2014**, *5* (1), 4445.
(30) Liljeström, V.; Seitsonen, J.; Kostiainen, M. A. Electrostatic Self-Assembly of Soft Matter Nanoparticle Cocrystals with Tunable Lattice Parameters. *ACS Nano* **2015**, *9* (11), 11278−11285.
(31) Beyeh, N. K.; Nonappa; Liljeström, V.; Mikkilä, J.; Korpi, A.; Bochicchio, D.; Pavan, G. M.; Ikkala, O.; Ras, R. H. A.; Kostiainen, M. A. Crystalline Cyclophane-Protein Cage Frameworks. *ACS Nano* **2018**, *12* (8), 8029−8036.
(32) Korpi, A.; Ma, C.; Liu, K.; Nonappa; Herrmann, A.; Ikkala, O.; Kostiainen, M. A. Self-Assembly of Electrostatic Cocrystals from Supercharged Fusion Peptides and Protein Cages. *ACS Macro Lett.* **2018**, *7* (3), 318−323.
(33) Uchida, M.; McCoy, K.; Fukuto, M.; Yang, L.; Yoshimura, H.; Miettinen, H. M.; LaFrance, B.; Patterson, D. P.; Schwarz, B.; Karty, J. A.; Prevelige, P. E., Jr. Modular Self-Assembly of Protein Cage Lattices for Multistep Catalysis. *ACS Nano* **2018**, *12* (2), 942−953.
(34) Zhou, K.; Zang, J.; Chen, H.; Wang, W.; Wang, H.; Zhao, G. On-Axis Alignment of Protein Nanocage Assemblies from 2D to 3D through the Aromatic Stacking Interactions of Amino Acid Residues. *ACS Nano* **2018**, *12* (11), 11323−11332.
(35) Sana, B.; Johnson, E.; Le Magueres, P.; Criswell, A.; Cascio, D.; Lim, S. The Role of Nonconserved Residues of Archaeoglobus Fulgidus Ferritin on Its Unique Structure and Biophysical Properties. *J. Biol. Chem.* **2013**, *288* (45), 32663−32672.
(36) Pulsipher, K. W.; Bulos, J. A.; Villegas, J. A.; Saven, J. G.; Dmochowski, I. J. A Protein-Protein Host-Guest Complex: Thermostable Ferritin Encapsulating Positively Supercharged Green Fluorescent Protein. *Protein Sci.* **2018**, *27* (10), 1755−1766.
(37) Swift, J.; Butts, C. A.; Cheung-Lau, J.; Yerubandi, V.; Dmochowski, I. J. Efficient Self-Assembly of Archaeoglobus Fulgidus Ferritin around Metallic Cores. *Langmuir* **2009**, *25* (9), 5219−5225.
(38) Tetter, S.; Hilvert, D. Enzyme Encapsulation by a Ferritin Cage. *Angew. Chem., Int. Ed.* **2017**, *56* (47), 14933−14936.
(39) Lawrence, M. S.; Phillips, K. J.; Liu, D. R. Supercharging proteins can impart unusual resilience. *J. Am. Chem. Soc.* **2007**, *129*, 10110−10112.
(40) Knubovets, T.; Osterhout, J. J.; Connolly, P. J.; Klibanov, A. M. Structure, Thermostability, and Conformational Flexibility of Hen Egg-White Lysozyme Dissolved in Glycerol. *Proc. Natl. Acad. Sci. U. S. A.* **1999**, *96* (4), 1262−1267.
(41) Hu, M.; Wang, J.; Peng, Q. Identification and Visualization of Cage-Shaped Proteins. *Bioinformatics* **2007**, *23* (24), 3400−3402.
(42) Schoonen, L.; Maassen, S.; Nolte, R. J. M.; van Hest, J. C. M. Stabilization of a Virus-Like Particle and Its Application as a Nanoreactor at Physiological Conditions. *Biomacromolecules* **2017**, *18* (11), 3492−3497.

DOI: 10.1021/acs.nanolett.9b01148
Nano Lett. 2019, 19, 3918−3924